small NANO MICRO

Bacteria

DOI: 10.1002/smll.200701164

Functional Fe_3O_4/TiO_2 Core/Shell Magnetic Nanoparticles as Photokilling Agents for Pathogenic Bacteria

*Wei-Jen Chen, Pei-Jane Tsai, and Yu-Chie Chen**

***A** photokilling approach for pathogenic bacteria is demonstrated using a new type of magnetic nanoprobe as the photokilling agent. In addition to their magnetic property, the nanoprobes have other features including a photocatalytic property and the capacity to target bacteria. The nanoprobes comprise iron oxide/titania (Fe_3O_4@TiO_2) core/shell magnetic nanoparticles. As dopamine molecules can self-assemble onto the surface of the titania substrate, dopamine is used as the linker to immobilize succinic anhydride onto the surfaces of the Fe_3O_4@TiO_2 nanoparticles. This is followed by the immobilization of IgG via amide bonding. We demonstrate that the IgG–Fe_3O_4@TiO_2 magnetic nanoparticles not only have the capacity to target several pathogenic bacteria, but they also can effectively inhibit the cell growth of the bacteria targeted by the nanoparticles under irradiation of a low-power UV lamp within a short period. Staphylococcus saprophyticus, Streptococcus pyogenes, and antibiotic-resistant bacterial strains, such as multiantibiotic-resistant S. pyogenes and methicillin-resistant Staphylococcus aureus (MRSA), are used to demonstrate the feasibility of this approach.*

Keywords:
- bacteria
- core/shell materials
- magnetic properties
- nanoparticles
- photochemistry

1. Introduction

Titania materials are widely used in various research fields due to their several unique features.[1–9] For example, titania beads have been known as effective adsorbents specific for phosphorylated peptides,[1–4] and nanocrystalline TiO_2 electrodes have been applied in the research of solar cells.[5] The ability of titania in photocatalytic reduction is applied in metal reduction to remove heavy metals from wastewater.[6] Furthermore, titania materials also have antimicrobial activities. Previous studies have demonstrated that titania materials can inhibit the cell growth of microorganisms via photochemical reactions.[7–9] However, these materials have no selectivity for specific microorganisms. Additionally, gold nanoparticles[10,11] and magnetic nanoparticles[12–15] have been used as either antibiotic agents or bacterial capture probes.

We have demonstrated that immunoglobulin G (IgG)-bound magnetic nanoparticles can recognize several pathogenic bacterial strains, including *Staphylococcus aureus*, *Staphylococcus saprophyticus*, and *Streptococcus pyogenes*, using pseudo-immune interactions.[16] The recognition by nanoprobes of pathogenic bacteria is based on pseudo-immune interactions between the Fc sites of IgG molecules and the binding proteins on the surfaces of these bacteria. IgG-bound magnetic nanoparticles have broadband affinity for pathogenic bacteria, which have binding affinities with the Fc site of IgG molecules.

Herein, we further extend the application of this type of affinity magnetic probe to inhibit the cell growth of bacteria by giving the probes a photocatalytic feature. That is, we immobilize a titania shell on the surface of magnetic nanoparticles prior to binding with IgG. Titania is known to

[*] W.-J. Chen, Prof. Y.-C. Chen
Department of Applied Chemistry
National Chiao Tung University
Hsinchu 300 (Taiwan)
Fax: (+886) 3-5131527
E-mail: yuchie@mail.nctu.edu.tw
Prof. Y.-C. Chen
Institute of Molecular Science
National Chiao Tung University
Hsinchu 300 (Taiwan)
Prof. P.-J. Tsai
National Laboratory Animal Center
National Applied Research Laboratories
Taipei 115 (Taiwan)

have the capacity to adsorb electron-donating bidentate enediol compounds, such as dopamine, onto its surface.[17–24] When mixing dopamine with iron oxide/titania (Fe_3O_4@TiO_2) core/shell magnetic nanoparticles, dopamine will self-assemble on the surface of the shell of the nanoparticles using its bidentate enediol. The surface amines on the dopamine-bound magnetic nanoparticles can serve as functional groups for further modification with succinic anhydride. Then IgG can be readily bound onto the surface of the nanoparticles via amide bonding using carbodiimide as the coupling reagent. The generated IgG-bound magnetic nanoparticles then possess multiple features including magnetic properties, the capacity to target several pathogenic bacteria, and antimicrobial activity under irradiation by UV light. In addition to *S. saprophyticus* and *S. pyogenes*, antibiotic-resistant bacterial strains, such as multiantibiotic-resistant *S. pyogenes* and methicillin-resistant *S. aureus* (MRSA), were also used as samples for examination.

2. Results and Discussion

Scheme 1 shows the fabrication steps of IgG–Fe_3O_4@TiO_2 magnetic nanoparticles. A thin layer of silicate is first immobilized on the bare iron oxide nanoparticles followed by coating with another layer of titania. As a result of the chelating capability of titania with dopamine, dopamine molecules are proposed to readily attach onto the surfaces of the Fe_3O_4@TiO_2 nanoparticles by simply suspending the nanoparticles with a dopamine solution. To confirm the binding of dopamine onto the surfaces of the Fe_3O_4@TiO_2 nanoparticles, gold nanoparticles with negatively charged protection groups were added to two solutions containing unmodified Fe_3O_4@TiO_2 nanoparticles and dopamine-immobilized Fe_3O_4@TiO_2 nanoparticles.

Figure 1 presents a photograph of these two solutions with a magnet attached to the outside of the sample vials. The solution in the left-hand vial, which contains gold nanoparticles and unmodified Fe_3O_4@TiO_2 nanoparticles, retains its red color. However, the solution in the vial on the right, which contains gold nanoparticles and dopamine-immobilized Fe_3O_4@TiO_2 nanoparticles, becomes colorless because the nanoparticles are aggregated on the wall of the vial by an external magnetic field. The results indicate that the dopamine molecules are attached to the surfaces of the Fe_3O_4@TiO_2 nanoparticles. As a result, the dopamine-immobilized magnetic nanoparticles are net positively charged and are able to interact with negatively charged gold nanoparticles. The dopamine–Fe_3O_4@TiO_2 magnetic nanoparticle–gold nanoparticle conjugates can be readily aggregated by an external magnetic field. However, without the attachment of dopamine on their surfaces, the unmodified Fe_3O_4@TiO_2 nanoparticles do not interact with the negatively charged gold nanoparticles. This is understandable, because the isoelectric point of titania is ≈5.2,[25] which results in unmodified Fe_3O_4@TiO_2 having a net negative charge in deionized water. The negatively charged Fe_3O_4@TiO_2 nanoparticles repel the negatively charged gold nanoparticles.

We then reacted the dopamine-immobilized Fe_3O_4@TiO_2 nanoparticles with succinic anhydride. After carboxylate terminals were generated on the surfaces of the magnetic nanoparticles, IgG molecules could be readily bound to the nanoparticles through amide bonding. The binding capacity of IgG on the beads was estimated as ≈0.8 nmol mg^{-1} (IgG/nanoparticles) by absorption spectrometry. We also used protein G, which can bind with the Fc site on IgG, to interact with the IgG–Fe_3O_4@TiO_2 nanoparticles and to determine the orientation of IgG on the particles. We found that 0.55 nmol of protein G was captured by 1 mg of IgG–Fe_3O_4@TiO_2 nanoparticles. That is, ≈68.7% of the IgG molecules on the surface of the nanoparticles are available for binding with their target molecules.

The generated IgG–Fe_3O_4@TiO_2 nanoparticles have two functions: the targeting capacity for bacteria and photocatalytic activity. To examine whether the Fe_3O_4@TiO_2 nanoparticles still possessed photocatalytic activity after their

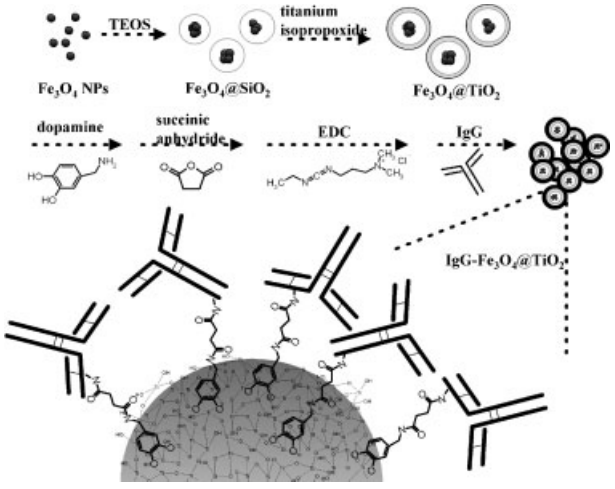

Scheme 1. Preparation steps for fabricating IgG-Fe_3O_4@TiO_2 magnetic nanoparticles.

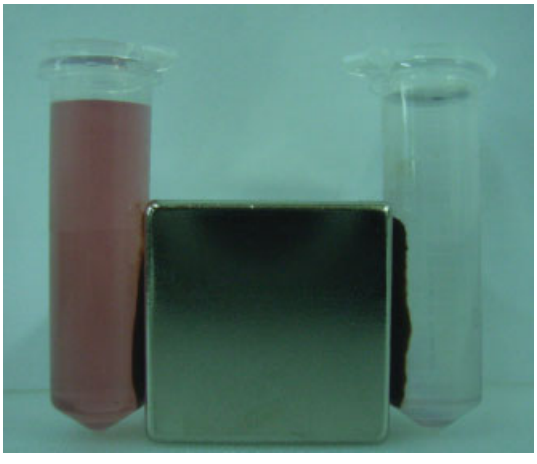

Figure 1. Photograph of a vial containing gold nanoparticles and unmodified Fe_3O_4@TiO_2 nanoparticles (left) and a vial containing unmodified gold nanoparticles and dopamine-immobilized Fe_3O_4@TiO_2 nanoparticles (right). A magnet was attached to the outside of these two vials.

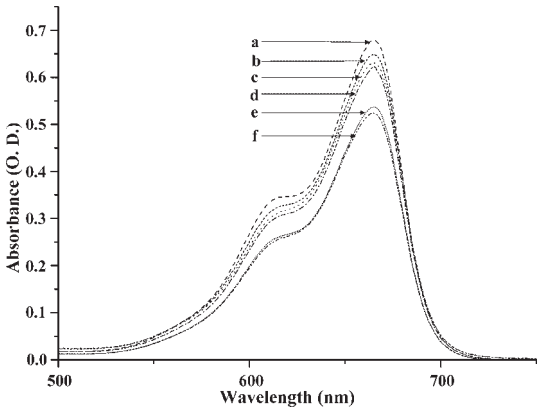

Figure 2. Absorption bands of methylene blue (10^{-5} M, 10 mL), which were obtained in the absence of nanoparticles in the dark (band a) and under illumination by UV light for 1 h (band d), in the presence of IgG–Fe_3O_4@TiO_2 nanoparticles (1 mg) in the dark (band b) and under illumination by UV light ($\lambda_{max} \approx 306$ nm) for 1 h (band e), and in the presence of Fe_3O_4@TiO_2 nanoparticles (1 mg) in the dark (band c) and under illumination by UV light for 1 h (band f).

surfaces were immobilized with IgG, we employed methylene blue to examine the photocatalytic reaction. It is known that methylene blue decomposes in the presence of photocatalytic materials such as titania under illumination by UV light ($\lambda_{max} \approx 306$ nm). The absorption bands a and d in Figure 2 were obtained from the sample containing methylene blue in the dark and under illumination by UV light for 1 h. The intensity of absorption band d is lower than that of band a due to photodecomposition. That is, methylene blue can be destroyed solely by UV light. However, the level of the decrease of methylene blue (band d) is much less than that obtained from the methylene blue sample containing Fe_3O_4@TiO_2 nanoparticles (1 mg; band f). Absorption band f was obtained from the supernatant by incubating methylene blue and Fe_3O_4@TiO_2 nanoparticles under illumination by UV light for 1 h. Absorption band c is its corresponding control result obtained by incubating the same sample in the dark for 1 h. The intensity of absorption band c is lower than that of band a because Fe_3O_4@TiO_2 nanoparticles can adsorb methylene blue, which results in a decrease of the concentration of methylene blue in the supernatant. When our IgG–Fe_3O_4@TiO_2 nanoparticles (1 mg) were added to the methylene blue solution under illumination by UV light for 1 h, the intensity of the supernatant (band e) was higher than that of band f. It seems that the photocatalytic capability of IgG–Fe_3O_4@TiO_2 might be slightly worse than that of Fe_3O_4@TiO_2. However, when examining the corresponding absorption spectrum of the supernatant obtained by incubating methylene blue with IgG–Fe_3O_4@TiO_2 nanoparticles in the dark for 1 h (band b), we found that the intensity of the absorption band is higher than that of absorption band c (Fe_3O_4@TiO_2 control). As the experiment was carried out in the dark, the decrease in the absorption band of methylene blue is contributed to by the adsorption capacity of the nanoparticles for methylene blue. Based on the results shown by bands b and c, we concluded that the adsorption capacity of Fe_3O_4@TiO_2 nanoparticles for methylene blue is better than that of IgG–Fe_3O_4@TiO_2 nanoparticles. The results also show that the difference between the intensity of the absorption bands e and f arises from the different adsorption capacity of these two types of nanoparticles for methylene blue. The findings indicate that the photocatalytic activity of Fe_3O_4@TiO_2 nanoparticles and IgG–Fe_3O_4@TiO_2 nanoparticles is similar.

Table 1. The trapping capacity of IgG–Fe_3O_4@TiO_2 magnetic nanoparticles for several pathogenic bacteria.

Bacterial strains	Trapping capacity [cfu mg^{-1}]
S. pyogenes M9022434	$(2.21 \pm 0.24) \times 10^7$
S. pyogenes M9141204	$(3.54 \pm 0.14) \times 10^9$
S. saprophyticus	$(2.61 \pm 0.06) \times 10^8$
S. pyogenes JRS4	$(1.19 \pm 0.34) \times 10^9$
S. aureus	$(1.09 \pm 0.09) \times 10^9$
S. pyogenes JRS75	$(2.24 \pm 1.43) \times 10^3$
MRSA	$(1.71 \pm 1.13) \times 10^3$

In addition, we investigated the targeting capability of the IgG–Fe_3O_4@TiO_2 nanoparticles for several pathogenic bacteria. Table 1 presents the trapping capacity of IgG–Fe_3O_4@TiO_2 magnetic nanoparticles for seven bacterial strains: *S. pyogenes* M9022434, *S. pyogenes* M9141204, *S. saprophyticus*, *S. pyogenes* JRS 4, *S. aureus*, *S. pyogenes* JRS 75, and MRSA. The trapping capacity of the nanoparticles for *S. pyogenes* M9022434, *S. saprophyticus*, *S. pyogenes* JRS 4, and *S. pyogenes* M9141204 is 10^7–10^9 cfu mg^{-1}

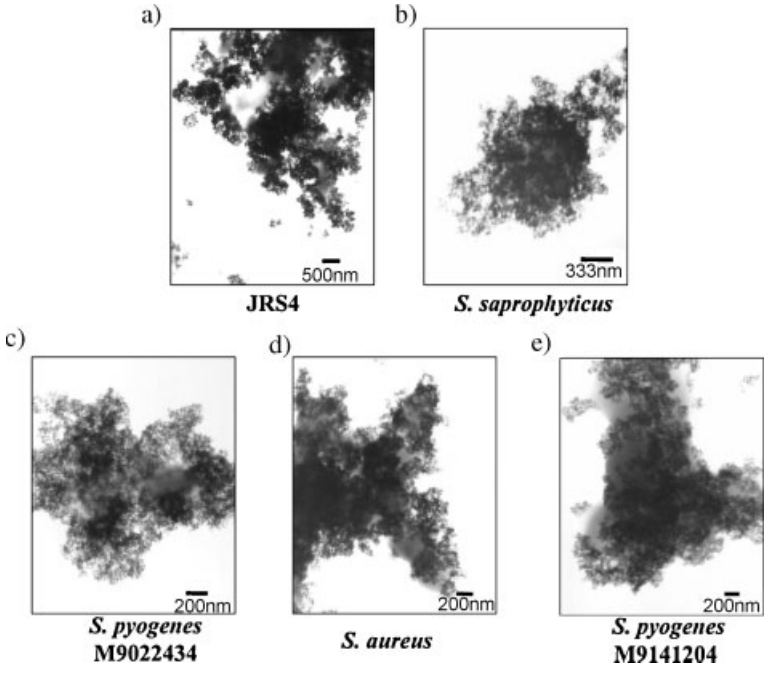

Figure 3. TEM images of a) *S. pyogenes* JRS 4, b) *S. saprophyticus*, c) *S. pyogenes* M9022434, d) *S. aureus*, and e) *S. pyogenes* M9141204 interacting with IgG–Fe_3O_4@TiO_2 magnetic nanoparticles followed by magnetic separation.

(cfu = colony-forming unit). However, the trapping capacity for *S. pyogenes* JRS 75 and MRSA is apparently much lower ($\approx 10^3$ cfu mg^{-1}), which indicates that the affinity probes have weak interactions with these two strains of bacteria. In addition to MRSA, both *S. pyogenes* M9022434 and M9141204 are multiantibiotic-resistant bacteria, and *S. pyogenes* JRS 75 is a mutated bacterial strain.[26] The results show that our IgG–Fe_3O_4@TiO_2 magnetic nanoparticles have the capacity of trapping antibiotic-resistant *S. pyogenes* M9022434 and M9141204. However, the trapping capacity of the nanoparticles for both *S. pyogenes* JRS 75 and MRSA is poor among these bacterial strains. This poor trapping capacity of the nanoparticles for JRS 75 is due to the mutation of the M protein in JRS 75. Thus, it was not surprising to obtain such results. Furthermore, it is understandable that the magnetic nanoparticles have weak interactions with MRSA, because it has been demonstrated that Pls protein on the surface of MRSA can sterically hinder the binding of protein A with IgG.[27]

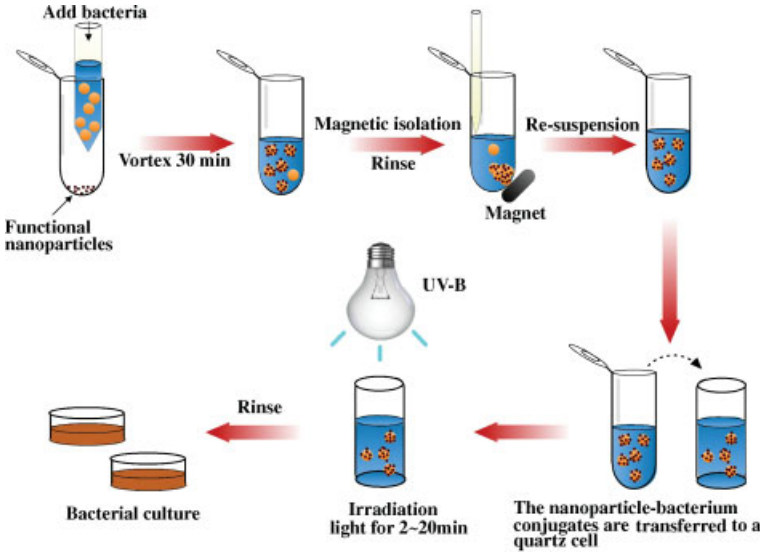

Scheme 2. Schematic image to show the steps followed in the photokilling experiment.

Figure 3a–e presents transmission electron microscopy (TEM) images of *S. pyogenes* JRS 4, *S. saprophyticus*, *S. pyogenes* M9022434, *S. aureus*, and *S. pyogenes* M9141204 interacting with IgG–Fe_3O_4@TiO_2 nanoparticles followed by magnetic separation. The cell walls of the bacteria trapped by the magnetic nanoparticles are fully covered with the nanoparticles, thus confirming that the nanoparticles can interact with these bacteria. The results demonstrate that the IgG–Fe_3O_4@TiO_2 magnetic nanoparticles have the capacity to target several pathogenic bacteria.

We further employed the nanoparticles as photokilling agents for bacteria. Scheme 2 shows the steps of photokilling using the IgG–Fe_3O_4@TiO_2 magnetic nanoparticles as the photokilling agents under UV light irradiation. The nanoparticles were allowed to interact with their target bacteria for 30 min, followed by magnetic isolation. The nanoparticle–bacterium conjugates were rinsed several times and were then resuspended in a solution of tryptic soy broth with yeast (TSBY). The solution was irradiated with UV light ($\lambda_{max} = 306$ nm) for 2–20 min. Then the nanoparticle–bacterium conjugates were isolated and diluted, followed by culture on TSBY agar.

Figure 4a–e shows plots of the survival ratio (%) of *S. pyogenes* M9141204, *S. aureus*, *S. pyogenes* M9022434, *S. saprophyticus*, and *S. pyogenes* JRS4 as a function of illumination time by UV light. The plots marked with filled triangles and empty triangles present the control results obtained by incubating the bacterial samples in the dark and under illumination by UV light for 2–20 min, respectively. The survival ratio in the control results remains >80% as the illumination time is extended to 20 min. However, the survival ratio of the plots marked with filled squares obtained in the presence of IgG–Fe_3O_4@TiO_2 magnetic nanoparticles is dramatically decreased to <20% as the illumination time is increased to 20 min. The results indicate that the cell growth of the bacteria targeted by the IgG–Fe_3O_4@TiO_2 magnetic nanoparticles is effectively inhibited in the presence of the nanoparticles under illumination by UV light. Table 2 summarizes the survival ratio for these bacterial samples. More than ≈80% of the bacteria can be effectively inhibited. Furthermore, this approach is effective for

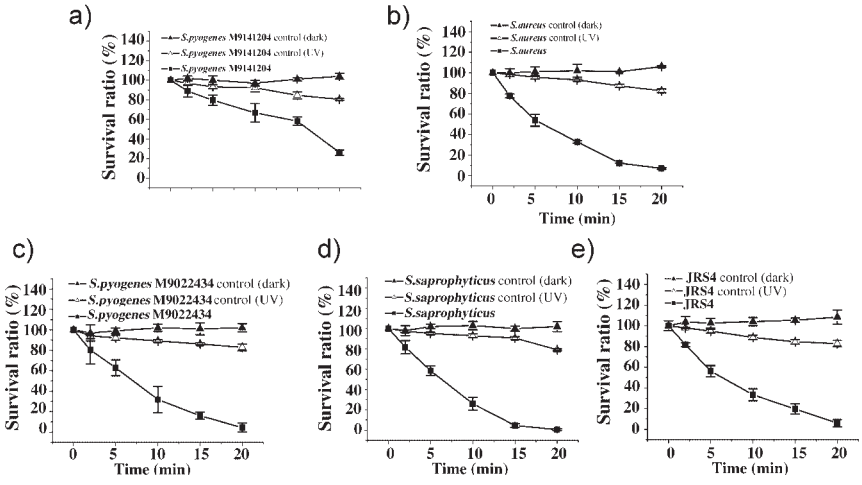

Figure 4. Plots of the survival ratio (%) of a) *S. pyogenes* M9141204, b) *S. aureus*, c) *S. pyogenes* M9022434, d) *S. saprophyticus*, and e) *S. pyogenes* JRS4 as a function of the illumination time by UV light. The plots marked with filled triangles and empty triangles are the control results obtained by incubating the bacteria in the dark and under UV light irradiation for 2–20 min, respectively, in the absence of the nanoparticles. The plot marked with filled squares was obtained by irradiating the bacteria with UV light for 2–20 min in the presence of IgG–Fe_3O_4@TiO_2 nanoparticles. The cell concentration of these bacterial samples (1 mL) was 10^9–10^{10} cfu mL^{-1}.

small NANO MICRO

Table 2. Survival ratio (%) of the bacteria obtained after irradiation by UV light for 20 min.

Bacterial strains	Survival ratio (N/N_0)[a]	
	Control [%]	IgG–Fe_3O_4@TiO_2 [%]
JRS4	82.78	5.95
S. saprophyticus	79.15	0.51
S. pyogenes M9022434	82.87	4.45
S. pyogenes M9141204	80.45	26.09
S aureus	82.40	7.13

[a]N = number of survival bacteria; N_0 = number of original bacteria.

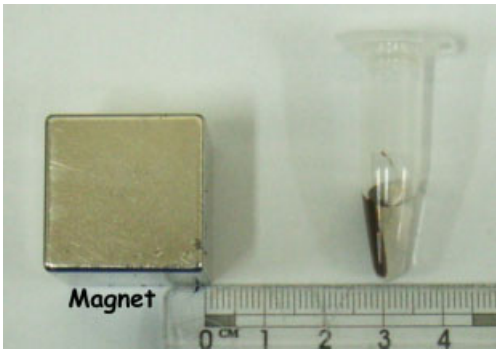

Figure 5. Photograph showing a magnet placed at a distance within 3 cm of the vial containing bacteria and magnetic nanoparticles.

several antibiotic-resistant bacterial strains. Compared with previous studies,[28–30] the light power and the time required to inhibit the cell growth of bacteria are much less in our approach. Additionally, the conjugates of IgG–Fe_3O_4@TiO_2 nanoparticles and bacteria can be readily driven to a specific spot based on their magnetic property. We have found that the nanoparticle–bacterium conjugates can be driven to aggregate on a vial wall by a magnet within a distance of ≈3 cm from the vial (Figure 5). This feature can be potentially employed in testing in vivo. If the conjugates can be aggregated on a specific spot when carrying out in vivo tests, the light irradiation can be specifically focused on the spot and therefore the damage to the normal cells resulting from the UV light can be reduced. This is the unique advantage of using magnetic nanoparticles as the targeting probe. However, further studies carried out in vivo are required to demonstrate this point.

3. Conclusions

We have demonstrated that IgG–Fe_3O_4@TiO_2 nanoparticles are effective nanoprobes for inhibiting the cell growth of several pathogenic bacteria under illumination by UV light. We combined two unique features of titania, its photocatalytic activity and its ability to self-assemble dopamine onto its surface, in the design of the photokilling agents. The illumination time required in this approach is shorter than that involved in previous studies. The improvement can be attributed to two main factors. First, the size of the nanoprobes contributed to the highly efficient energy transfer from UV light to the target bacteria. Second, the targeting capacity of the nanoprobes for several bacteria also results in the effectiveness of the cell growth inhibition of these bacteria. Additionally, the nanoprobes have the capacity to target several pathogenic bacteria, including antibiotic-resistant strains. Although the transmission of UV light is limited, this approach should potentially be suitable for the treatment of cutaneous infections.

4. Experimental Section

Reagents and materials: Iron(III) chloride hexahydrate was purchased from Riedel–de Haën (Seelze, Germany). Iron(II) chloride tetrahydrate, aqueous ammonia, tetraethyl orthosilicate (TEOS), nitric acid, 3-hydroxytyramine hydrochloride, and succinic anhydride were purchased from Fluka (Germany). Hydrochloric acid, isopropyl alcohol, and dimethyformamide (DMF) were obtained from J. T. Baker (Phillipsburg, NJ). Ethanol was purchased from Showa (Tokyo, Japan). Titanium(IV) isopropoxide, 2-(*N*-morpholino)ethanesulfonic acid (MES) hydrate, *N*-(3-dimethylaminopropyl)-*N*'-ethylcarbodiimide hydrochloride (EDC), methylene blue, IgG from human serum, and protein G were purchased from Sigma (St Louis, MO). Tryptic soy broth (TSB) and granulated agar were purchased from Becton Dickinson (Franklin Lakes, NJ). Yeast extract was obtained from Alpha Bioscience (Baltimore, MD).

Preparation of iron oxide magnetic nanoparticles: Both $FeCl_2$ (2 g) and $FeCl_3$ (5.4 g) were dissolved in aqueous hydrochloric acid (2 M, 25 mL), and the air in the mixture was eliminated using a pump. The mixture was stirred for 10 min under nitrogen followed by the addition of aqueous ammonia (28%, 40 mL) with stirring. After 1 h, the generated iron oxide nanoparticles were rinsed with deionized water two or three times.

Preparation of titania-coated iron oxide (Fe_3O_4@TiO_2) magnetic nanoparticles: The nanoparticles generated above (0.2 g) were rinsed with ethanol three times and then resuspended in ethanol (40 mL) under sonication for 1 h. Aqueous ammonia (4.5 mL), deionized water (3.75 mL), and TEOS (0.1 mL) were added in sequence to the suspension. The mixture was sonicated for 1 h followed by vortex mixing for another 8 h. The silica-modified nanoparticles were isolated by magnetic separation and were rinsed with ethanol two or three times. The nanoparticles were resuspended in ethanol (40 mL) followed by refluxing at 60 °C for 12 h. After rinsing with deionized water, the generated nanoparticles were resuspended in deionized water (40 mL) and the suspension was acidified with nitric acid (0.5 M, 0.22 mL)/deionized water (124.78 mL) solution. The suspension was heated at 60 °C, and a solution containing titanium isopropoxide (15 μL) and 2-propanol (11.985 mL) was slowly added to the mixture under stirring for 6 h. *TEOS, titanium isopropoxide, and DMF are toxic. They should be handled with care by preparing the reagents in a hood and wearing gloves if necessary*. The generated Fe_3O_4@TiO_2 magnetic nanoparticles were rinsed with deionized water twice. Direct contact of the nanoparticles with the hands should be avoided as the nanoparticles have photocatalytic activity.

Preparation of IgG-bound magnetic nanoparticles: The Fe_3O_4@TiO_2 magnetic nanoparticles (6 mg) were vortexed for 1 h

with dopamine (10 mM, 3 mL) prepared in deionized water. *Dopamine is irritating to the eyes, respiratory system, and skin and should be handled with care*. After rinsing with DMF, the dopamine-bound Fe_3O_4@TiO_2 magnetic nanoparticles (6 mg) were reacted with succinic anhydride (200 mg mL^{-1}, 5 mL) prepared in DMF for 6 h under nitrogen protection. The nanoparticles were then isolated and rinsed with DMF (3 mL) three times. They were reacted with EDC (50 mg mL^{-1}, 3 mL) for 10 min followed by rinsing with MES buffer (pH 6.3, 20 mL) three times. The nanoparticles were then reacted for 24 h with IgG (8.35×10^{-7} M, 15 mL) prepared in MES buffer (pH 6.3).

Preparation of bacterial samples: *Staphylococcus saprophyticus*, erythromycin, chloramphenicol-resistant *Streptococcus pyogenes* (M9022434), erythromycin, clindamycin, chloramphenicol-resistant *S. pyogenes* (M9141204), *Staphylococcus aureus*, and methicillin-resistant *S. aureus* (MRSA) were collected from patients at the General Tzu-Chi Hospital, Hualien, Taiwan. *S. pyogenes* JRS 75 and JRS 4 were kind gifts from Dr. J. R. Scott (Emory University School of Medicine). *S. pyogenes* JRS 75 was obtained by mutating the *S. pyogenes* JRS 4 strain.[26] These bacteria were cultured in TSBY (15 mL), which was prepared by dissolving TSB (24 g) and yeast (4 g) in deionized water (800 mL). After incubation overnight at 37 °C, the bacterial cells were centrifuged at 6000 rpm for 10 min and then washed with sterilized water (2×10 mL). The desired bacterial concentration was adjusted by measuring the optical density at 600 nm. It was checked by plating serial dilutions of the samples on TSBY agar, which was prepared by dissolving TSB (24 g), yeast (4 g), and granulated agar (12.8 g) in deionized water (600 mL), and counting the colony-forming units after incubation overnight at 37 °C. In an experiment using live bacteria as samples, the bacterial cells were used directly without heat treatment. Similarly, the desired bacterial concentration was prepared based on the measurement of optical density at 600 nm.

Estimation of the bacterial trapping capacity of IgG-bound Fe_3O_4@TiO_2 nanoparticles: IgG-bound Fe_3O_4@TiO_2 magnetic nanoparticles were rinsed with TSBY prior to trapping experiments. The nanoparticles (2.57 mg) were then vortexed with bacterial samples (1 mL) with a cell concentration of 10^9–10^{10} cfu mL^{-1} for 30 min, and the experiment was shielded from light by wrapping the sample vials with aluminum foil. The nanoparticle–bacteria conjugates were isolated by magnetic separation followed by rinsing with TSBY (5×1 mL) and resuspension in TSBY. Then the nanoparticle–bacteria conjugate suspension (0.2 mL) was diluted with TSBY (0.8 mL). The capacity of the nanoparticles for bacteria was determined by diluting the suspension 5×10^6–5×10^7-fold before culture on TSBY agar in the dark. The number of cells was then determined by plate counting.

Photokilling: Scheme 2 presents the steps in using IgG-bound Fe_3O_4@TiO_2 nanoparticles as photokilling agents for bacteria. The magnetic nanoparticles obtained were rinsed with TSBY prior to trapping experiments. The nanoparticles (2.57 mg) were vortexed for 30 min with bacterial samples (1 mL) with a cell concentration of 10^9–10^{10} cfu mL^{-1}. The nanoparticle–bacteria conjugates were isolated by magnetic separation followed by rinsing with TSBY (5×1 mL) and resuspension in TSBY. The nanoparticle–bacteria conjugate suspension (0.2 mL) was diluted with TSBY (0.8 mL) and irradiated with a UVB lamp ($\lambda_{max} \approx 306$ nm; G8T5E, Sankyo Denki, Japan, 0.412 mW cm^{-2}) for a given time (2–20 min). After irradiation, the suspension was diluted 5×10^4–5×10^5-fold prior to culture on TSBY agar plates. The bacterial cells were then counted after incubation overnight.

Instrumentation: TEM images were obtained with a JEOL microscope (2000FX, Japan). Absorption spectra were obtained by a Varian Cary 50 spectrophotometer (Melbourne, Australia).

Acknowledgements

We thank the National Science Council (NSC) of Taiwan and MOE-ATU (96W821G021 and 96W801H109) for supporting this research financially. We thank Shu-Jen Weng in the co-facility center at the National Central University (Taiwan), and Cheng-Tai Chen, Wei-Yu Chen, and Wei-Chieh Huang for their technical assistance in obtaining the TEM images. We also thank Prof. Yaw-Kuen Li (NCTU) for lending us the required equipment for bacterial culture.

[1] A. Sano, H. Nakamura, *Anal. Sci.* **2004**, *20*, 565–566.
[2] A. Sano, H. Nakamura, *Anal. Sci.* **2004**, *20*, 861–864.
[3] M. H. Pinkse, P. M. Uitto, M. J. Hilhorst, B. Ooms, A. J. R. Heck, *Anal. Chem.* **2004**, *76*, 3935–3943.
[4] C.-T. Chen, Y.-C. Chen, *Anal. Chem.* **2005**, *77*, 5912–5919.
[5] M. K. Nazeeruddin, A. Kay, I. Rodicio, R. Humphry-Baker, E. Mueller, P. Liska, N. Vlachopoulos, M. Graetzel, *J. Am. Chem. Soc.* **1993**, *115*, 6382–6390.
[6] M. R. Prairie, L. R. Evans, B. M. Stange, S. L. Martinez, *Environ. Sci. Technol.* **1993**, *27*, 1776–1782.
[7] S. Rana, J. Rawat, R. D. K. Misra, *Acta Biomater.* **2005**, *1*, 691–703.
[8] J. Rawat, S. Rana, R. Srivastava, R. D. K. Misra, *Mater. Sci. Eng. C* **2007**, *27*, 540–545.
[9] K. Page, R. G. Palgrave, I. P. Parkin, M. Wilson, S. L. P. Savin, A. V. Chadwick, *J. Mater. Chem.* **2007**, *17*, 95–104.
[10] J. Gil-Tomás, S. Tubby, I. P. Parkin, N. Narband, L. Dekker, S. P. Nair, M. Wilson, C. Street, *J. Mater. Chem.* **2007**, *17*, 3739–3746.
[11] W.-C. Huang, P.-J. Tsai, Y.-C. Chen, *Nanomedicine* **2007**, *2*, 777–787.
[12] J. Gao, L. Li, P.-L. Ho, G. C. Mak, H. Gu, B. Xu, *Adv. Mater.* **2006**, *18*, 3145–3148.
[13] H. Gu, P.-L. Ho, K. W. T. Tsang, L. Wang, B. Xu, *J. Am. Chem. Soc.* **2003**, *125*, 15702–15703.
[14] H. Gu, P.-L. Ho, K. W. T. Tsang, C.-W. Yu, B. Xu, *Chem. Commun.* **2003**, 1966–1967.
[15] Y.-S. Lin, P.-J. Tsai, M.-F. Weng, Y.-C. Chen, *Anal. Chem.* **2005**, *77*, 1753–1760.
[16] K.-C. Ho, P.-J. Tsai, Y.-S. Lin, Y.-C. Chen, *Anal. Chem.* **2004**, *76*, 7162–7168.
[17] T. Rajh, J. M. Nedeljkovic, L. X. Chen, O. Poluektov, M. C. Thurnauer, *J. Phys. Chem. B* **1999**, *103*, 3515–3519.
[18] T. Rajh, L. X. Chen, K. Lukas, T. Liu, M. C. Thurnauer, D. M. Tiede, *J. Phys. Chem. B* **2002**, *106*, 10543–10552.
[19] N. M. Dimitrijevic, Z. V. Saponjic, D. M. Bartels, M. C. Thurnauer, D. M. Tiede, T. Rajh, *J. Phys. Chem. B* **2003**, *107*, 7368–7375.
[20] L. Qingwen, W. Yiming, L. Guoan, *Mater. Sci. Eng. C* **2000**, *11*, 71–74.

[21] M. Niederberger, G. Garnweitner, F. Krumeich, R. Nesper, H. Cölfen, M. Antonietti, *Chem. Mater.* **2004**, *16*, 1202–1208.
[22] T. Rajh, Z. Saponjic, J. Liu, N. M. Dimitrijevic, N. F. Scherer, M. Arroyo-Vega, P. Zapol, L. A. Curtiss, M. C. Thurnauer, *Nano Lett.* **2004**, *4*, 1017–1023.
[23] L. de la Garza, Z. V. Saponjic, T. Rajh, N. M. Dimitrijevic, *Chem. Mater.* **2006**, *18*, 2682–2688.
[24] L. de la Garza, Z. V. Saponjic, N. M. Dimitrijevic, M. C. Thurnauer, T. Rajh, *J. Phys. Chem.* **2006**, *110*, 680–686.
[25] S. Watson, J. Scott, D. Beydoun, R. Amal, *J. Nanopart. Res.* **2005**, *7*, 691–705.
[26] M. Norgren, M. G. Caparon, J. R. Scott, *Infect. Immun.* **1989**, *57*, 3846–3850.
[27] K. Savolainen, L. Paulin, B. Westerlund-Wikstrom, T. J. Foster, T. K. Korhonen, P. Kuusela, *Infect. Immun.* **2001**, *69*, 3013–3020.
[28] T. Matsunaga, M. Okochi, *Environ. Sci. Technol.* **1995**, *29*, 501–505.
[29] A. G. Rincon, C. Pulgarin, N. Adler, P. Peringer, *J. Photochem. Photobiol. A* **2001**, *139*, 233–241.
[30] K. Sunada, T. Watanabe, K. Hashimoto, *J. Photochem. Photobiol. A* **2003**, *156*, 227–233.

Received: November 24, 2007
Published online: March 18, 2008

